Space-Domain Green's Function Approach to the Capacitance Calculation of Multiconductor Lines in Multilayered Dielectrics with Improved Surface Charge Modeling

WIM DELBARE AND DANIËL DE ZUTTER

Abstract—**An integral equation method for the calculation of capacitance and inductance matrices is presented. The method is suitable for multiconductor transmission lines embedded in a multilayered dielectric medium on top of a ground plane. Conductors of arbitrary polygonal cross section can be handled, as well as infinitely thin conductors. The method is new in two respects. The kernel of the integral equation is the space-domain Green's function of the layered medium. The accuracy of the solution is enhanced by using basis functions which exactly model the singular behavior of the charge density in the neighborhood of a conductor edge. Numerical examples show the accuracy of the calculations and the complexity of the configurations that can be treated.**

I. Introduction

IN THIS PAPER a new method will be described for the calculation of the capacitance and inductance matrices of multiconductor transmission lines embedded in a multilayered dielectric medium on top of a ground plane. In earlier publications this problem has been treated in different ways [1]–[3].

Recent approaches to the problem have been based on the solution of an integral equation with the Green's function as its kernel. The Green's function adopted as a kernel function is either the free-space Green's function [4] or the Green's function for the layered dielectric medium [5]–[9]. In the first case, polarization charges at the boundaries between the different dielectric layers of the medium have to be introduced as additional unknowns together with the actual surface charges on the conductors. In the second case only the surface charges themselves form the unknowns of the problem. In most cases the integral equation is solved using a point-matching technique [4].

The present method is also based on an integral equation for the surface charges on the conductors which is solved by the point-matching technique. It is original in two respects. In order to be able to solve for many layers, the Green's function for the layered medium is calculated. This avoids the problem of introducing additional polarization charges when using the free-space Green's function. In previous publications using the Green's function of the layered medium with many layers, the Green's function has been obtained by the method of separation of variables [6] or calculated in the spectral domain [7]–[9]. The use was restricted to infinitely thin strip conductors. In our approach, the Green's function is determined in the spectral domain, but its space-domain form is found by explicitly calculating its inverse Fourier transformation. This technique allows the treatment of thick conductors of arbitrary polygonal cross section. A second way in which our method differs from previously published approaches is the way in which the surface charges are expanded, using basis functions which explicitly account for the singularities of these charges near the edges of the conductors.

Numerical results for a number of configurations, some of which are also found in previous publications, illustrate the flexibility and accuracy of our method.

II. General Formulation of the Problem

The general geometry of the problem is shown in Fig. 1. An arbitrary number of conductors Nc are embedded in an arbitrary number of nonmagnetic dielectric layers Nd. The geometry is independent of the z direction, and the perfectly conducting ground plane is located at $y = 0$. The dielectric layers are numbered starting at the ground plane. The ith dielectric layer has a dielectric constant ϵ_i, and the y coordinate of the top of this layer is at $y = d_i$. Our approach will be valid for perfect conductors of arbitrary polygonal cross section as well as for infinitely thin perfectly conducting strips. Curved cross sections have to be approximated by a suitable polygon. We start from a representation of the potential $V(\boldsymbol{r})$ in terms of the surface

Manuscript received December 6, 1988; revised May 17, 1989. This work was supported by the National Fund for Scientific Research of Belgium.

The authors are with the Laboratory of Electromagnetism and Acoustics, University of Ghent, Sint-Pietersnieuwstraat 41, 9000-Ghent, Belgium.

IEEE Log Number 8929889.

0018-9480/89/1000-1562$01.00

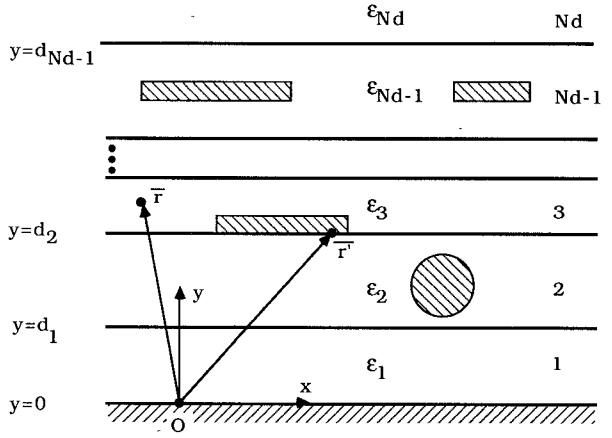

Fig. 1. Multiconductor transmission lines in a multilayered dielectric.

charge densities $\rho_j(\boldsymbol{r}')$ on each conductor surface S_j:

$$\sum_{j=1}^{Nc} \int_{S_j} \rho_j(\boldsymbol{r}') G(\boldsymbol{r}|\boldsymbol{r}')\, dr' = V(\boldsymbol{r}). \tag{1}$$

Here $G(\boldsymbol{r}|\boldsymbol{r}')$ represents the two-dimensional Green's function of the layered dielectric medium of Fig. 1.

In order to determine the capacitance matrix $\underline{C}$ of the configuration under study, (1) must be solved for $V(\boldsymbol{r})=1$ on each particular conductor surface S_i while being zero on the other conductors. The total charge q_j (per unit of length in the z direction) on conductor S_j corresponding to this potential distribution yields the element C_{ji} of the capacitance matrix.

The inductance matrix $\underline{L}$ is related to the vacuum capacitance matrix $\underline{C}_V$ by the simple formula $\underline{L}\cdot\underline{C}_V = \epsilon_0\mu_0$ [4]. The vacuum capacitance matrix $\underline{C}_V$ itself is the capacitance matrix of the conductor configuration under study but with all dielectrics replaced by free space.

The central problem addressed in this paper is the solution of the integral equation (1). Our method consists in expanding the ρ_j's in a suitable set of basis functions and in enforcing (1) at a limited number of points, i.e., the well-known point-matching technique. Before concentrating on the discretization of the surface charges and the solution of the integral equation, we will first describe how to determine the spatial Green's function G.

III. Green's Function in the Fourier Domain

Due to the uniformity of the dielectric medium in the x direction the Green's function $G(x, y|x', y')$ depends only upon the difference $|x-x'|$. Hence, in order to determine G, it will be sufficient to determine the potential due to a line charge located at $x'=0$ but with an arbitrary value of y', i.e., $G(x, y|0, y')$. To do this we introduce the Fourier transformation of all quantities with respect to the x coordinate. The Fourier-transformed Green's function $\tilde{G}(\alpha, y|0, y')$ is related to the original Green's function as follows:

$$\tilde{G}(\alpha, y|0, y') = \int_{-\infty}^{+\infty} G(x, y|0, y') e^{-j\alpha x}\, dx. \tag{2}$$

Using the above-cited property of the Green's function, $G(x, y|x', y')$ can easily be expressed in terms of the inverse Fourier cosine transformation of $\tilde{G}(\alpha, y|0, y')$ as follows:

$$G(x, y|x', y') = \frac{1}{\pi}\int_0^{+\infty} \tilde{G}(\alpha, y|0, y')\cos[\alpha(x-x')]\, d\alpha. \tag{3}$$

In what follows, the shorthand notation $\tilde{G}$ will be reserved for $\tilde{G}(\alpha, y|0, y')$. Before we give details on the calculation of $\tilde{G}$, it is important to remark that the height y' of the unit line charge which is the source of $\tilde{G}$ can be taken to coincide with one of the boundaries between the layers of the dielectric medium. Indeed, if this line charge were located within a layer, it would suffice to divide this layer into two new layers but with the same dielectric properties. In what follows we assume that the line charge is located at $y'=d_k$, i.e., at the boundary between the kth and the $(k+1)$th layer.

Within each dielectric layer $\tilde{G}$ satisfies

$$\frac{\partial^2\tilde{G}}{\partial y^2} - \alpha^2\tilde{G} = 0, \qquad i=1,2,\cdots,Nd. \tag{4}$$

The solution of (4) in the ith dielectric layer is

$$\tilde{G}(\alpha, y|0, y') = A_i e^{\alpha y} + B_i e^{-\alpha y}. \tag{5}$$

The coefficients A_i and B_i can be determined by applying the appropriate boundary conditions at the ground plane ($y=0$), at the interfaces between the layers, and at infinity ($y\to\infty$) and by applying the correct jump conditions at $y'=d_k$, i.e., the height at which the line source is located.

At $y=0$, the potential equals zero; consequently $A_1 = -B_1$. At the interfaces between subsequent layers $\tilde{G}$ and $\epsilon_r\,\partial\tilde{G}/\partial y$ must be continuous, expressing the continuity of the potential and of the normal component of the dielectric displacement vector $\boldsymbol{D}$. For $y\to\infty$ the potential must vanish. As $\tilde{G}(\alpha, y|0, y')$ is only calculated for $\alpha>0$ (3), this implies that A_{Nd} must be zero. In order to solve the set of equations for the A_i's and the B_i's in a numerically stable way, we proceed as follows. At $y=d_i$, i.e., the top of the ith layer, the unknown coefficients in this layer can be expressed in terms of the coefficients of the $(i+1)$th layer and vice versa:

$$\begin{bmatrix} A_i e^{2\alpha d_i} \\ B_i \end{bmatrix} = \underline{T}_i \cdot \begin{bmatrix} A_{i+1} e^{2\alpha d_{i-1}} \\ B_{i+1} \end{bmatrix}, \qquad i \neq k \tag{6}$$

and

$$\begin{bmatrix} A_{i+1} \\ B_{i+1} e^{-2\alpha d_{i+1}} \end{bmatrix} = \underline{U}_i \cdot \begin{bmatrix} A_i \\ B_i e^{-2\alpha d_i} \end{bmatrix}, \qquad i \neq k \tag{7}$$

where

$$\underline{T}_i = \begin{bmatrix} a_i e^{-2\alpha(d_{i+1}-d_i)} & b_i \\ b_i e^{-2\alpha(d_{i+1}-d_i)} & a_i \end{bmatrix}$$

$$\underline{U}_i = \begin{bmatrix} c_i & f_i \\ f_i e^{-2\alpha(d_{i+1}-d_i)} & c_i e^{-2\alpha(d_{i+1}-d_i)} \end{bmatrix} \tag{8}$$

$$a_i = (1/2)(1+\epsilon_{r,i+1}/\epsilon_{r,i}) \qquad b_i = (1/2)(1-\epsilon_{r,i+1}/\epsilon_{r,i})$$

$$c_i = (1/2)(1+\epsilon_{r,i}/\epsilon_{r,i+1}) \qquad f_i = (1/2)(1-\epsilon_{r,i}/\epsilon_{r,i+1}).$$

Instead of solving for the A_i's and B_i's, we solve for $A_i \exp(2\alpha d_i)$ and for $B_i \exp(-2\alpha d_i)$. In this way all growing exponentials are removed from $\underline{T}_i$ and $\underline{U}_i$ and numerical overflow is avoided in making products of $\underline{T}_i$ or $\underline{U}_i$ matrices. Repeated use of (6) allows us to express A_{k+1} and B_{k+1} in terms of B_{Nd}, while repeated use of (7) allows us to express A_k and B_k as a function of A_1. In order to determine the remaining unknowns A_1 and B_{Nd}, we only have to impose the appropriate jump conditions at $y' = d_k$, i.e., continuity of the potential and jump condition for the normal component of the dielectric displacement vector:

$$A_k e^{\alpha d_k} + B_k e^{-\alpha d_k} = A_{k+1} e^{\alpha d_k} + B_{k+1} e^{-\alpha d_k}$$

$$\epsilon_{r,k+1}\left(A_{k+1} e^{\alpha d_k} - B_{k+1} e^{-\alpha d_k}\right) - \epsilon_{r,k}\left(A_k e^{\alpha d_k} - B_k e^{-\alpha d_k}\right) = \frac{-1}{\alpha \epsilon_0}. \tag{9}$$

Solution of (9) in terms of A_1 and B_{Nd} and application of (6) and (7) finally lead to the solution for all A and B coefficients and hence to the potential $\tilde{G}$ everywhere.

IV. Green's Function in the Space Domain

To go from the Fourier domain to the space domain, the integral in (3) has to be calculated. To this end, the integration interval $[0, +\infty]$ is divided into two parts: $[0, T]$ and $[T, +\infty]$. In the first interval, the full expression for $\tilde{G}$ calculated above is used, while in the second interval $\tilde{G}$ is replaced by its asymptotic approximation. The constant T is determined as the value of the Fourier variable α for which the relative difference between $\tilde{G}$ and its asymptotic approximation is smaller than 10^{-6}. Integration over $[0, T]$ is performed using a Gaussian quadrature formula [12].

In order to obtain the asymptotic expression for $\tilde{G}$, only the slowest decreasing exponentials (as a function of α) occurring in $\underline{T}_i$ and $\underline{U}_i$ (8) are retained. The final result for the asymptotic expression of $\tilde{G}$ is given by

$$\lim_{\alpha \to \infty} \tilde{G} = \tilde{G}_\infty = \sum_{i=1}^{4} C_i \frac{e^{-\alpha Y_i}}{\alpha} = \sum_{i=1}^{4} \tilde{G}_\infty^{(i)}. \tag{10}$$

The expressions for the constants C_i and the distances Y_i, as well as a physical interpretation of these distances, are given in the Appendix. However, it is important to note that Y_1 simply represents the distance in the y direction between the source point and the observation point. Hence, this distance can become zero, which is not the case for Y_2, Y_3, and Y_4. The four contributions to $\tilde{G}_\infty$ in (10) can be integrated analytically over the interval $[T, +\infty]$:

$$\frac{1}{\pi}\int_T^{+\infty} C_i \frac{e^{-\alpha Y_i}}{\alpha} \cos\left[\alpha(x-x')\right] d\alpha = \frac{C_i}{2\pi}\left[E_1(\gamma) + E_1(\gamma^*)\right] = G_\infty^{(i)}$$

$$\gamma = T\left[Y_i + j(x-x')\right]. \tag{11}$$

In what follows we write the sum of the four terms $G_\infty^{(i)}$ as G_∞:

$$G_\infty = \sum_{i=1}^{4} G_\infty^{(i)}. \tag{12}$$

In (11), E_1 represents the exponential integral [10]. For the case where Y_1 becomes zero, the integration over $[T, +\infty]$ can be expressed in terms of the cosine integral Ci [10]:

$$\frac{1}{\pi}\int_T^{+\infty} C_1 \frac{\cos\left[\alpha(x-x')\right]}{\alpha} d\alpha = \frac{-C_1}{\pi}\,\mathrm{Ci}\left(T|x-x'|\right) = G_\infty^{(1)}(Y_1 = 0). \tag{13}$$

V. Discretization of the Surface Charges

The unknown charge distribution $\rho_j(\boldsymbol{r}')$ on each conductor is expanded in basis functions. To this end each side of a polygon is divided into a number of elementary intervals. In the inner intervals, such as AB (Fig. 2), linear basis functions are used:

$$\rho(t) = x_i(1-t) + x_{i+1}t, \qquad 0 \leqq t \leqq 1 \tag{14}$$

where t is proportional to the arc length along an elementary interval. The coefficients x_i and x_{i+1} are the unknown coefficients of the basis functions and correspond to the charge densities in the endpoints of the interval.

In the outer intervals near the edges, such as EF, the first terms of a series expansion which accurately models the singular behavior of the charge distribution in the neighborhood of an edge are used [11]. In this case, the charge distribution takes the form

$$\rho(t) = x_1 t^{\nu-1} + x_2 t^{\nu}, \qquad \nu > 0;\ 0 \leqq t \leqq 1 \tag{15}$$

where t is proportional to the distance to the edge. The sum $x_1 + x_2$ corresponds to the charge density in the nonsingular endpoint of the interval. The value of ν is

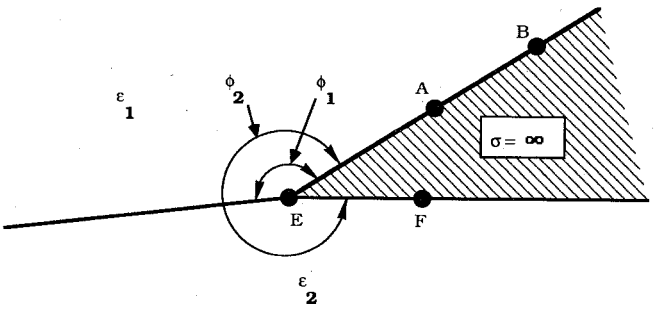

Fig. 2. Discretization of the surface charges.

obtained from a formula which was derived by Meixner [11]:

$$\frac{\epsilon_1-\epsilon_2}{\epsilon_1+\epsilon_2}=\frac{\sin\nu\phi_2}{\sin\nu(2\phi_1-\phi_2)}. \tag{16}$$

The meanings of the quantities ϵ_1, ϵ_2, ϕ_1, and ϕ_2 are made clear in Fig. 2.

VI. Solution of the Integral Equation and Self-Patch Calculation

Using the space-domain Green's function found in Section IV and starting from the discretization of the surface charges adopted above, the contributions to the integral equation (1) from every elementary surface charge interval must be evaluated for each point-matching point in which (1) is enforced. We must distinguish between the case where the matching point does not belong to the charge interval we have to integrate over, and the case where it does belong to that interval, i.e., the so-called self-patch contribution. For the non-self-patch contributions simple Gaussian quadrature can be used to perform the integration. The self-patch contribution, however, needs special attention and will be discussed below. The matching points are chosen in the endpoints of all elementary charge intervals and also in the middle of the outer intervals of each side of the conducting polygons, i.e., the intervals containing the edges of the conductors. The number of equations obtained in this way exceeds the number of unknowns, but only marginally. This set of equations is solved in the least-squares sense.

We now turn to the self-patch calculation. In order to illustrate the problem, we restrict ourselves to the self-patch calculation for an elementary charge interval near the edge of a conductor. Furthermore, we suppose that this interval is parallel to the x axis and that the matching point is located in the middle of the interval. The situation corresponds to the one shown in Fig. 2 for the interval EF. For different situations the calculations proceed in an analogous way, although they are less intricate in the case of an inner interval such as AB (see Fig. 2).

The self-patch contribution to (1), from the interval EF described above, is

$$\frac{1}{\pi}\int_{EF}\rho(x')\,dx'\int_0^\infty \tilde{G}\cos[\alpha(x-x')]\,d\alpha. \tag{17}$$

As in (15), we introduce the local t coordinate to describe ρ and again divide the α integration interval into two parts, i.e., $[0,T]$ and $[T,+\infty]$. Hence (17) takes the form

$$L\int_0^1\left(x_1t^{\nu-1}+x_2t^{\nu}\right)(G_T+G_\infty)\,dt$$

$$G_T=\frac{1}{\pi}\int_0^T\tilde{G}\cos\alpha L(\tau-t)\,d\alpha$$

$$G_\infty=\sum_{i=2}^{4}G_\infty^{(i)}+\frac{1}{\pi}\int_T^\infty C_1\frac{e^{-\alpha Y_1}}{\alpha}\cos\alpha L(\tau-t)\,d\alpha. \tag{18}$$

In these equations L represents the length of EF and τ is the t value of the point-matching point x. As in the non-self-patch case, no problem arises for the contribution coming from G_T. We first calculate G_T using Gaussian quadrature, and the integration over t is performed using Gauss–Jacobi quadrature, which handles the $t^{\nu-1}$ and t^{ν} singularities exactly. The Gauss–Jacobi quadrature is based on the generalized Jacobi polynomials $P_n^{(\alpha,\beta)}$ [10]. As explained in Section IV, the contribution from G_∞ consists of four parts: $G_\infty^{(i)}$, $i=1,2,3,4$ (12). For $i=2$, 3, and 4, Y_i never vanishes. Hence, the integration over t can proceed in the same way as for G_T. The only real difficulty is due to the contribution which would normally arise from $G_\infty^{(1)}$. This contribution depends upon Y_1, i.e., the distance in the y direction between the source point and the point-matching point. In the case of the self-patch contribution from EF, Y_1 is zero. Looking at (13), the corresponding value of $G_\infty^{(1)}$ still exists under the form of a cosine integral, but while integrating over the self-patch interval, x will become equal to x' and the cosine integral becomes infinite. In order to obtain the correct contribution to the self-patch term in the integral equation, we still write $G_\infty^{(1)}$ under the form of a cosine integral, but in order to integrate over t, the integration interval is divided in two parts: $[0,\tau]$ and $[\tau,1]$:

$$-\frac{LC_1}{\pi}\int_0^\tau\left(x_1t^{\nu-1}+x_2t^{\nu}\right)\mathrm{Ci}[LT(\tau-t)]\,dt$$

$$-\frac{LC_1}{\pi}\int_\tau^1\left(x_1t^{\nu-1}+x_2t^{\nu}\right)\mathrm{Ci}[LT(t-\tau)]\,dt. \tag{19}$$

The cosine integral has a logarithmic singularity at $t=\tau$. Hence, the first integral exhibits a logarithmic singularity at $t=\tau$ and a t^κ singularity at $t=0$, where $\kappa=\nu$ or $\kappa=\nu-1$. The second integral only exhibits a logarithmic singularity at $t=\tau$. The final integration is performed in the following way. In both cases the cosine integral is written as the sum of its logarithmic singularity and the remaining regular part. If we now also divide the interval $[0,\tau]$ into two equal parts, we only need to calculate integrals which have a t^κ singularity, a logarithmic singularity, or no singularity at all in the endpoints of the integration interval. These integrations are performed using Gauss–Jacobi, Gauss–Laguerre, or simple Gaussian quadrature [12].

VII. Numerical Examples

A. Thin Microstrip Line

As a first example we start with the analysis of a very simple configuration, i.e., the thin microstrip line shown in Fig. 3. This analysis is used to illustrate the accuracy of the method. For different values of the ratio W/H, where W is the width of the strip and H is the substrate thickness, Table I shows the comparison between the characteristic impedance values obtained with our method, the results from Wei *et al.* [4] based on the free-space Green's function, the results from the well-known formulas of Gupta [1], and those from more recent and more accurate formulas by Hammerstad and Jensen [13]. Our results are ob-

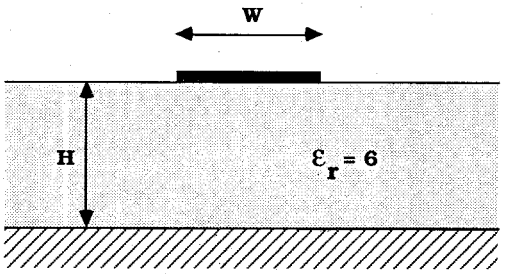

Fig. 3. Thin microstrip line.

TABLE I
CHARACTERISTIC IMPEDANCES FOR THE THIN MICROSTRIP LINE

W/H	Our results	Gupta	Wei	Hammerstad
0.4	90.3204	90.1907	90.2785	90.3339
0.7	72.7372	72.6731	73.9626	72.7516
1.0	61.8422	61.5907	62.8109	61.8397
2.0	42.2676	42.3945	42.9980	42.2600
4.0	26.4429	26.5168	26.9709	26.4593
10.	12.7132	12.7164	12.9961	12.7198

tained by using 20 subsections on the strip. The results of Wei *et al.* [4] are obtained by using 12 subsections on the strip, 15 subsections at the dielectric interface between $-2W$ and $-W/2$, and another 15 subsections at the dielectric interface between $W/2$ and $2W$. At small W/H values, differences of up to 2 percent are found between our results and those from Wei, and although the differences between Gupta and Hammerstad are very small, our method is closer to the more exact results by Hammerstad.

B. Three Line Bus in a Layered Dielectric

This is an example of a more complex geometry, shown in Fig. 4. For the charge modeling, we used ten subsections on each horizontal side and three subsections on each vertical side of the strips. Table II gives the results for the capacitance matrix $\underline{C}$ and for the inductance matrix $\underline{L}$. The results of our charge modeling are exemplified in Fig. 5. This figure shows the calculated charge distribution along the four sides of the second strip. For this particular case, all strips are at the same potential of 1 V.

C. Geometry Containing a Conductor of Circular Cross Section

The final example is taken from [4] in order to illustrate the ability of our method to handle conductors of circular cross section (see Fig. 6). For the charge modeling, we used 14 subsections on conductors 1 and 2. The circular cross section was approximated by an octagon. As each side of the octagon was divided into three subsections, a total of 24 subsections was used for the third conductor. Table III shows a comparison between our results and those obtained by Wei *et al.* [4]. Results are given for the capacitance matrix $\underline{C}$ and for the inductance matrix $\underline{L}$.

VIII. CONCLUSION

In this paper we have described an improved method for determining the capacitance and inductance matrices of a multiconductor transmission line in a multilayered dielec-

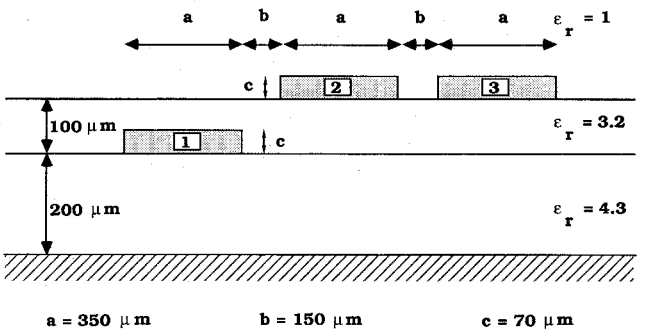

Fig. 4. Three line bus in a layered dielectric.

TABLE II
CAPACITANCE AND INDUCTANCE MATRIX FOR THE CONFIGURATION OF FIG. 4

$$\underline{C} = \begin{bmatrix} 142.09 & -21.765 & -0.8920 \\ -21.733 & 93.529 & -18.098 \\ -0.8900 & -18.097 & 87.962 \end{bmatrix} \text{ (pF/m)}$$

$$\underline{L} = \begin{bmatrix} 277.73 & 87.758 & 36.770 \\ 87.758 & 328.60 & 115.77 \\ 36.770 & 115.77 & 337.98 \end{bmatrix} \text{ (nH/m)}$$

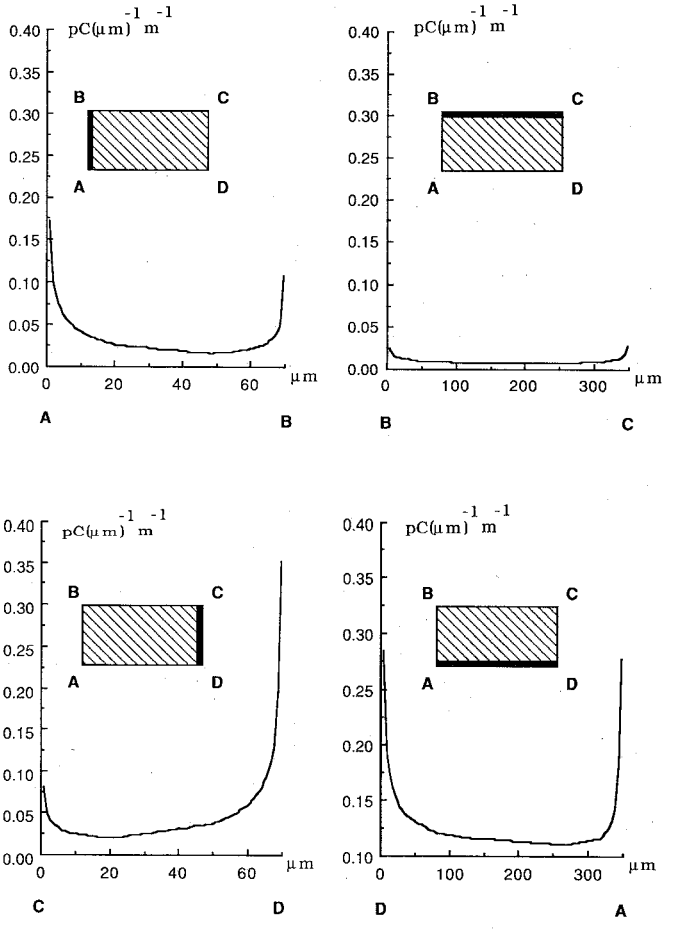

Fig. 5. Charge distributions along the sides of the second strip of Fig. 4.

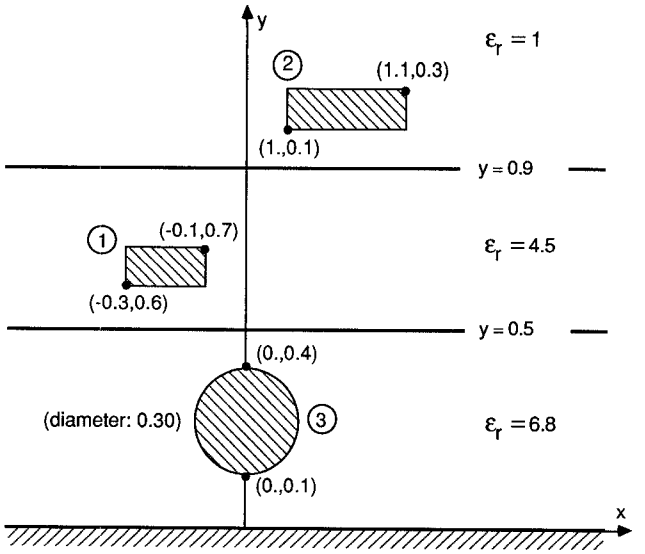

Fig. 6. Multiconductor transmission line containing a conductor of circular cross section.

TABLE III
CAPACITANCE AND INDUCTANCE MATRIX ELEMENTS FOR THE CONFIGURATION OF FIG. 6

	Our results	Cao Wei et al.	Units
C_{11}	125.86	124.4	pF/m
C_{12}	-13.125	-13.00	pF/m
C_{13}	-69.555	-68.25	pF/m
C_{22}	34.101	33.40	pF/m
C_{23}	-7.1818	-7.196	pF/m
C_{33}	357.62	352.3	pF/m
L_{11}	491.90	496.5	nH/m
L_{12}	198.88	199.6	nH/m
L_{13}	117.50	118.3	nH/m
L_{22}	612.83	616.3	nH/m
L_{23}	76.781	77.28	nH/m
L_{33}	229.94	233.1	nH/m

tric medium. By explicitly calculating the Green's function in the space domain, it became possible to handle conductors of arbitrary polygonal cross section. We have demonstrated how the inverse Fourier transformation of the spectral Green's function can be handled in order to determine the self-patch contributions to the integral equation correctly. Another novelty of our approach resides in the fact that the singularities of the charges near the edges of the conductors are modeled exactly. The particular basis functions used in this paper ensure quick convergence of the numerical results, even with a small number of subsections per circumference. The selected examples demonstrated both the accuracy and the flexibility of our method. Finally, it should be emphasized that the use of the Green's function of the layered medium results in reduced calculation times. This is essential for practical design purposes. Special care is taken to be able to handle structures which are large in the x direction. It is clear that our method can easily be extended to the stripline case, i.e., the case where the multilayered medium is bounded by two perfectly conducting ground planes.

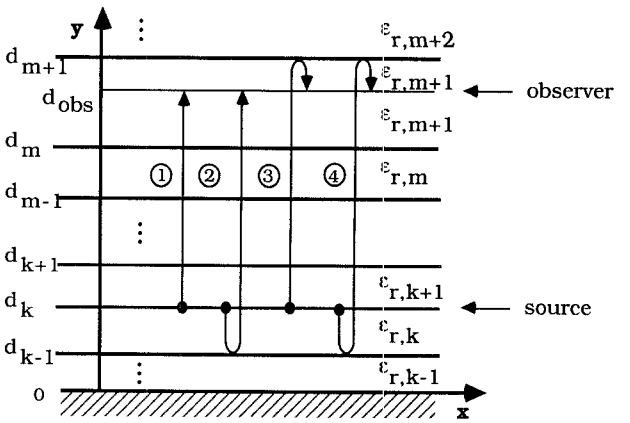

Fig. 7. The four waves of the asymptotic approximation.

APPENDIX

The differential equation (4) and the corresponding boundary conditions in the spectral domain have the form of the equations governing the behavior of voltage and current along a cascade of transmission lines [9]. The voltage at each point of the line results from a superposition of a direct wave and a number of multiply reflected waves. The amplitude of the waves is multiplied by a damping factor $e^{-\alpha d}$, where d is the total distance traveled by the wave in the y direction.

The four waves that are taken into account in the asymptotic approximation are depicted in Fig. 7. The coefficients C_i in (10) are

$$C_1 = \frac{1}{2\epsilon_0 \epsilon_{r,k}} \prod_{i=k}^{m} \frac{2\epsilon_{r,i}}{\epsilon_{r,i} + \epsilon_{r,i+1}} \tag{A1}$$

$$C_2 = C_1 \frac{\epsilon_{r,k} - \epsilon_{r,k-1}}{\epsilon_{r,k} + \epsilon_{r,k-1}} \tag{A2}$$

$$C_3 = C_1 \frac{\epsilon_{r,m+1} - \epsilon_{r,m+2}}{\epsilon_{r,m+1} + \epsilon_{r,m+2}} \tag{A3}$$

$$C_4 = C_1 \left(\frac{\epsilon_{r,k} - \epsilon_{r,k-1}}{\epsilon_{r,k} + \epsilon_{r,k-1}} \right) \left(\frac{\epsilon_{r,m+1} - \epsilon_{r,m+2}}{\epsilon_{r,m+1} - \epsilon_{r,m+2}} \right). \tag{A4}$$

The distances Y_i in (10) are the distances depicted on Fig. 7, i.e.,

$$\begin{aligned} Y_1 &= d_{obs} - d_k \\ Y_2 &= d_{obs} - d_k + 2(d_k - d_{k-1}) \\ Y_3 &= d_{obs} - d_k + 2(d_{m+1} - d_{obs}) \\ Y_4 &= d_{obs} - d_k + 2(d_k - d_{k-1}) + 2(d_{m+1} - d_{obs}). \end{aligned} \tag{A5}$$

REFERENCES

[1] K. C. Gupta, R. Garg, and I. J. Bahl, *Microstrip Lines and Slotlines*. Dedham, MA. Artech House, 1979.

[2] C. D. Taylor, G. N. Elkhouri, and T. E. Wade, "On the parasitic capacitances of multilevel parallel metallization lines," *IEEE Trans. Electron Devices*, vol. ED-32, pp. 2408-2415, Nov. 1985.

[3] R. Pregla and S. Nokes, "Calculation of the capacitance of thick microstrip using a variational expression," *Arch. Elek. Übertragung*, Band 29, pp. 125-128, 1975.

[4] C. Wei, R. F. Harrington, J. R. Mautz, and T. K. Sarkar, "Multiconductor transmission lines in multilayered dielectric media," *IEEE Trans. Microwave Theory Tech.*, vol. MTT-32, pp. 439–450, Apr. 1984.
[5] W. T. Weeks, "Calculation of coefficients of capacitance of multiconductor transmission lines in the presence of a dielectric interface," *IEEE Trans. Microwave Theory Tech.*, vol. MTT-18, pp. 35–43, Jan. 1970.
[6] A. Farrar and A. T. Adams, "Multilayer microstrip transmission lines," *IEEE Trans. Microwave Theory Tech.*, vol. MTT-22, pp. 889–891, Oct. 1974.
[7] R. Marqués, M. Horno, and F. Medina, "A new recurrence method for determining the Green's function of planar structures with arbitrary anisotropic layers," *IEEE Trans. Microwave Theory Tech.*, vol. MTT-33, pp. 424–428, May 1985.
[8] N. K. Das and D. M. Pozar, "A generalized spectral-domain Green's function for multilayer dielectric substrate with application to multilayer transmission lines," *IEEE Trans. Microwave Theory Tech.*, vol. MTT-35, pp. 326–335, Mar. 1987.
[9] R. Crampagne, M. Ahmadpanah, and J.-L. Guiraud, "A simple method for determining the Green's function for a large class of MIC lines having multilayered dielectric structures," *IEEE Trans. Microwave Theory Tech.*, vol. MTT-26, pp. 82–87, Feb. 1978.
[10] M. Abramowitz and I. A. Stegun, Eds., *Handbook of Mathematical Functions*, National Bureau of Standards (Applied Mathematics Series—55), Dec. 1965.
[11] Josef Meixner, "The behavior of electromagnetic fields at edges," *IEEE Trans. Antennas Propagat.*, vol. AP-20, no. 4, July 1972.
[12] N. Bakhavlov, *Méthodes Numériques*, 2nd ed. Moscow, U.S.S.R.: Mir, 1976.
[13] E. Hammerstad and O. Jensen, "Accurate models for microstrip computer-aided design," in *IEEE MTT-S Int. Microwave Symp. Dig.* (Washington DC), 1980, pp. 407–409.

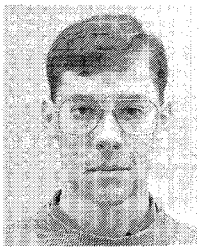

Wim Delbare was born in Ghent, Belgium, on November 1, 1962. He received the degree in electrical engineering from the University of Ghent in 1985. He is currently a research assistant of the Belgian National Foundation for Scientific Research working toward the Ph.D. degree in electrical engineering at the University of Ghent. His research work concerns circuit modeling of interconnections in high-speed digital circuits.

✠

Daniël De Zutter was born in Eeklo, Belgium, on November 8, 1953. He received the degree of electrical engineering from the University of Ghent, Belgium, in 1976. From September 1976 to September 1984 he was a research and teaching assistant in the Laboratory of Electromagnetism and Acoustics (LEA) at the same university. In October 1981 he obtained the Ph.D. degree there and in the spring of 1984 he completed a thesis leading to a degree equivalent to the French "Aggrégation" or the German "Habilitation".

His earlier scientific work dealt with the electrodynamics of moving media and with hyperthermia. At present he works at the LEA as a Senior Research Associate of the National Fund for Scientific Research of Belgium. He is leading a research group on high-speed/high-frequency electronics. His major research topics are interconnections and packaging.